Buckling Load and Performance Assessment of Train Roof Stiffened Panels: A Numerical Study

Ridwan Ridwan[1,*], Nur Candra Dana Agusti[1], Sudarno Sudarno[1], Sutrisno Sutrisno[1], Elia Larasati[1], Aditya Rio Prabowo[2]

[1] Department of Mechanical Engineering, Universitas Merdeka Madiun, Madiun 63133, Indonesia
[2] Department of Mechanical Engineering, Universitas Sebelas Maret, Surakarta 57126, Indonesia
ridwan@unmer-madiun.ac.id

Abstract. In recent years, there have been significant advancements in the development of new regulations aimed at ensuring the structural integrity of passenger rail car interiors, specifically their ability to withstand compression. These regulations have been adapting to accommodate the inclusion of rail equipment that conforms to alternative standards, with the ultimate goal of achieving safety levels. A crucial change in these regulations involves the shift from using traditional draft lines to applying proof loads along the collision load path. This adjustment requires passenger equipment designed with alternative methods to demonstrate their ability to withstand specific loading scenarios, particularly those designed to resist buckling loads. This article provides a comprehensive examination of this shift in regulations, focusing on the use of various innovative design enhancements of stiffened panel used in train roof using finite element method. These enhancements come in different configurations, including T-shaped and Hat Stiffeners, as well as a novel hybrid design combining elements of both T-shaped and Hat Stiffeners. Through a thorough analysis, the performance of these new stiffener designs is carefully evaluated, with the primary aim of determining how well they meet the strength criteria set by traditional equipment. The results of this study revealed distinct differences among various panel types. Notably, the T-Hat panel outperformed the others, demonstrating the highest resistance to buckling forces. This is highlighted by a substantial difference of approximately 67.5% when compared to the T-type panel and a significant 34.0% difference when compared to the Hat-type panel.

Keywords: Train Roof, Stiffened Panel, Buckling Analysis, Ultimate Strength, Finite Element Method.

1 Introduction

Train transportation plays a pivotal role in today's society, serving as a cornerstone of efficient and sustainable mobility [1]. In an era marked by increasing urbanization and environmental concerns, trains offer a compelling solution to the challenges of congestion and pollution. They are the lifeblood of mass transit systems in many ma-

A. Pradipta et al. (eds.), *Proceedings of the 2nd International Conference on Railway and Transportation 2023 (ICORT 2023)*, Advances in Engineering Research 231,
https://doi.org/10.2991/978-94-6463-384-9_15

jor cities, providing a reliable, safe, and cost-effective mode of transportation for millions of commuters daily. Additionally, trains play a crucial role in the global supply chain, facilitating the movement of goods across vast distances with unmatched efficiency. As societies strive for greener alternatives, trains stand as a beacon of sustainability, emitting far fewer greenhouse gases per passenger or ton of cargo compared to other forms of transportation. In this age of rapid technological advancement, the integration of high-speed rail, digital ticketing, and advanced safety systems ensures that train transportation remains indispensable for the interconnected world we live in today [2].

The growing need for increased train transportation has unfortunately led to a rise in train-related catastrophes, including collisions, buckling incidents, and fires [3-4]. As train networks expand to accommodate higher passenger and cargo volumes, the risk of accidents also escalates. Train collisions, whether between two trains or at rail crossings, can have devastating consequences, leading to loss of life and property damage. Buckling incidents, often exacerbated by extreme weather conditions, can disrupt rail services and pose safety hazards. Ngamkhanong et al. [5] showed that s straightforward concrete pathway can substantially raise the temperature at which buckling occurs by approximately 25%. Moreover, the risk of fires on trains and near rail infrastructure is a pressing concern, given the flammable nature of certain cargo and the complex machinery involved. Study conducted by Bi et al. [6] highlighted that the occurrence of a high-speed train carriage fire often follows the characteristics of a ventilation-controlled fire. The fire-resistant qualities of window glass play a crucial role in ensuring the fire safety of high-speed trains. These catastrophes not only endanger lives but also result in significant economic losses and environmental damage. Addressing these challenges is imperative to ensure the continued growth of train transportation while prioritizing safety and resilience in the face of potential disasters [7]. This underscores the need for ongoing investment in modernizing rail infrastructure, implementing advanced safety measures, and enhancing emergency response protocols to mitigate the impact of such catastrophes and ensure the sustainability of train transportation in the future.

In this study, a fresh and pioneering design for the roof of train passenger was conceived and scrutinized to determine its resistance to buckling under different loads. The technique employed involves the application of finite element analysis, complemented by benchmarking efforts aimed at bolstering the reliability of the findings. Furthermore, the deformation model of the design was subject to thorough analysis.

2 Buckling Phenomenon

Buckling is a critical mechanical phenomenon that can have serious implications in various engineering fields. It occurs when a structural component, such as a column or beam, becomes unstable and suddenly deforms under compressive loads. The analysis of buckling is essential in engineering design and structural integrity assessments. Engineers utilize mathematical models and simulations to predict the critical load at which buckling is likely to occur and assess the factors that contribute to instability.

Understanding buckling behavior is crucial in ensuring the safety and performance of structures ranging from buildings and bridges to aerospace components. Engineers employ sophisticated techniques such as finite element analysis (FEA) to simulate buckling scenarios, allowing for the optimization of designs to prevent or mitigate buckling-related failures. By carefully studying buckling phenomena and conducting thorough buckling analyses, engineers can develop structures that are not only robust and durable but also safer for the people who rely on them.

Kirchhoff introduced the simplest plate theory in the 1850s, known as Kirchhoff theory or classical thin plate theory (CPT). According to this theory:

1. Plate deflection is considered small, less than the plate's thickness.
2. During bending, the middle plane of the plate remains in the neutral surface and doesn't undergo stretching.
3. Plate sections can rotate during bending to be normal to the neutral surface, with no distortion, resulting in stresses and strains proportional to the distance from the neutral surface.
4. Shearing forces are disregarded, and loads are solely resisted by bending moments within the plate elements.
5. The plate's thickness is not significantly greater than its other dimensions.

When examining buckling in a thin rectangular plate subjected to biaxial compression using Kirchhoff or classical thin plate theory (CPT), the governing equation can be found in reference [8].

$$D\left(\frac{\partial^4 w}{\partial x^4}+2\frac{\partial^4 w}{\partial x^2 \partial y^2}+\frac{\partial^4 w}{\partial y^4}\right)+N_x\frac{\partial^2 w}{\partial x^2}+N_y\frac{\partial^2 w}{\partial y^2}=0 \tag{1}$$

In this context, w refers to the transverse deflection, and D represents the plate's flexural rigidity. D can be expressed as

$$\mathrm{D}=\frac{\mathrm{Eh}^3}{12(1-\mathrm{v}^2)} \tag{2}$$

Here, h represents the plate's thickness, E stands for Young's Modulus, and v denotes the Poisson's ratio.

$$\mathrm{D}\frac{\partial^2 \mathrm{w}}{\partial \mathrm{n}^2}+\mathrm{Dv}\frac{\partial^2 \mathrm{w}}{\partial \mathrm{s}^2}\mp\frac{\mathrm{K}_\mathrm{r}^\mathrm{m}}{\mathrm{L}}\frac{\partial \mathrm{w}}{\partial \mathrm{n}}=0 \tag{3}$$

with

$$\mathrm{N}\frac{\partial \mathrm{w}}{\partial \mathrm{n}}+\mathrm{D}\frac{\partial^2 \mathrm{w}}{\partial \mathrm{n}^3}+(2-\mathrm{v})\mathrm{D}\frac{\partial^3 \mathrm{w}}{\partial^2 \partial \mathrm{n}}\pm\mathrm{K}_\mathrm{l}^\mathrm{m}\mathrm{w}=0 \tag{4}$$

In accordance with references [9-10], n and s denote the direction perpendicular to the edge and the direction parallel to the edge, respectively.

For plate buckling, in the case of slender rectangular plates subjected to compressive loads, buckling occurs once the applied load reaches a specific critical threshold.

For rectangular plates that are supported on all sides, the formula for the critical buckling load is as follows.

$$N_{cr} = \frac{k_c \pi^2 D}{b^2} \tag{5}$$

Where D can be calculated based on Equation (2). Here, a represents the length of the plate when unloaded, while b represents the length when loaded. The buckling coefficient, k_c, depends on the aspect ratio a/b and the specific type of support at the plate edges (boundary condition).

3 Materials and Methods

3.1 Benchmarking Study

Quinn et al. [11] conducted experimental buckling tests on stiffened panels with two different specimens. The specimen geometry and the dimension are shown in Fig. 1. Specimen A had three longitudinal stringers of 590 mm length, 28 mm height and 2.8 mm thickness on the plate surface, spaced 167 mm apart. Specimen B had five sub-stiffeners of 8.7 mm height and 1.4 mm thickness between the longitudinal stringers, as seen in Fig. 1b. The plate thickness of both specimens was 2.2 mm and they were made of Aluminium Alloy 2024-T351.

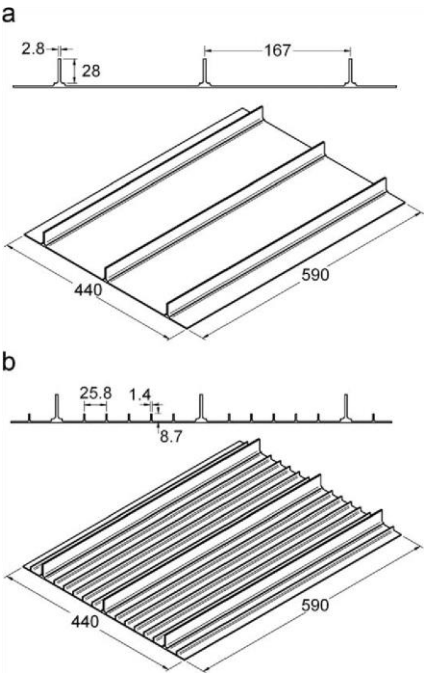

Fig. 1. The dimension on the stiffened panel as presented in [11].

A hydraulic testing machine with a capacity of 500 kN was used for the experimental tests. Clamped boundary conditions were provided by a reinforced epoxy resin base of 42 mm thickness at each end of the specimen loading. Strain gauges were used to measure the initial plate buckling and post-buckling collapse. Two calibrated displacement transducers, one on each side of the specimen, were used to measure specimen displacement. This study only uses Specimen B as a benchmarking study.

In this research, the study involved replicating the buckling tests conducted by Quinn et al. [11] on stiffened panels through nonlinear finite element analysis. The analysis was conducted utilizing the ANSYS commercial finite element software [12]. Specimen B, along with longitudinal stringers and sub-stiffeners, were simulated using shell elements. Subsequently, the deformation (plasticity) and the relationship between load and displacement will be compared to the outcomes of the experimental tests.

Regrettably, in Quinn et al.'s experimental test, there was no mention of the material properties for Aluminum Alloy 2024-T35. Consequently, this study assumed and employed the material properties of Aluminum Alloy 2024-T3, which include a density of 2780 kg/m³, a Young's modulus of 73.4 GPa, and a Poisson's ratio of 0.33 [13-14], as detailed in Table 1. The total mass of the specimens did not exhibit a significant disparity when compared to the experimental data, as presented in Table 1. Specifically, for Specimen B, the total mass was 1.993 kg, which closely aligned with the experimental data at 1.968 kg, resulting in a mass percentage difference of less than 1.27% compared to the experimental data.

Table 1. Mass comparison of the samples.

		Mass [kg]	Mass Difference [kg]	Mass Percentage Difference [%
Quinn et al. [11]	Specimen B	1968	-	-
Current study	Specimen B	1993	+0.025	+1.27

3.2 Results

Extensive mesh convergence investigations were meticulously conducted in the course of this study with the explicit objective of ascertaining the most suitable mesh size for the model under investigation. This thorough examination was undertaken to guarantee that fluctuations in the mesh size had no discernible influence on the outcomes of the analysis. The process of selecting an appropriate mesh size was consistently characterized by the intricate and delicate balance that needed to be struck between the pursuit of precision, the need to maintain computational efficiency within acceptable timeframes, and the judicious allocation of valuable computational resources. These critical considerations regarding mesh size optimization, and their inherent trade-offs, are extensively discussed and elucidated in the pertinent literature sources, notably as emphasized in references [15-18].

A total of 5 different mesh sizes, ranging from 5 mm to 20 mm, were chosen. Fig. 2 displays the selected mesh sizes alongside the load versus displacement curves. It's

apparent that the load versus displacement curve for all mesh sizes closely matched the experimental data [11]. Mesh sizes between 5 mm and 15 mm yielded the most accurate results. Notably, the best agreement with the experimental data for the ultimate panel collapse load was achieved when using a 10 mm mesh size for Specimen B, as shown in Fig. 2. Specimen B exhibited ultimate panel collapse loads of 257.1 kN, which were slightly higher than the experimental data of 255.0 kN, with errors not exceeding 2.8%. This suggests a strong alignment between the results and the experimental data.

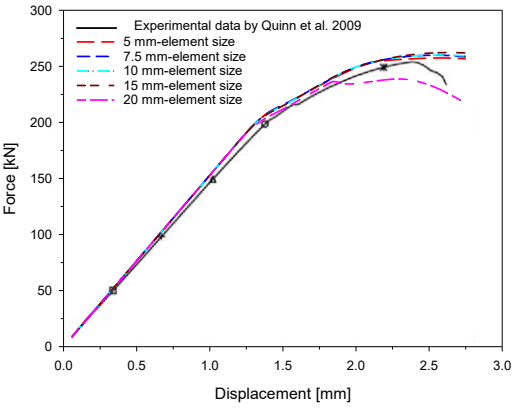

Fig. 2. Force versus displacement curve of the stiffened panel subjected to buckling load.

3.3 Extended Study

In order to facilitate an in-depth and comprehensive investigation, this research was primarily centered on the rigorous examination of the stiffened panel, which, for reference, featured a plate with dimensions measuring 500 mm in width and 1000 mm in length, along with a uniform thickness of 5 mm. This meticulous study encompassed an extensive exploration of a multitude of configurations and dimensions, all with the overarching goal of optimizing the design of train roofs.

The scope of this exploration included diverse panel types, specifically the T-type, Hat-type, and T-Hat type panels, each of which was subjected to thorough analysis and evaluation. As part of the research's commitment to providing precise and detailed information, it is noteworthy that the specifications and precise measurements of the stiffened panel have been meticulously documented and presented in Fig. 3, with all measurements being denoted in millimeters (mm) for clarity and precision.

3.4 Boundary Condition

The boundary conditions governing the behavior of the stiffened plate, as visually depicted in Fig. 4, provide a comprehensive overview of the structural constraints and controlled deformations. At one end of the plate, a fixed support has been meticulous-

ly employed, meticulously ensuring that both translational and rotational movements are thoroughly constrained. This results in the complete immobilization of Ux, Uy, Uz, Rx, Ry, and Rz, all uniformly set to 0, which effectively secures that end against any conceivable motion or rotation. Conversely, at the opposing end of the plate, a similar level of rigor has been applied to establish boundary conditions. In a mirror image of the constraints at the first end, this second end also enforces restrictions on translation and rotation. Specifically, Uy, Uz, Rx, Ry, and Rz are all uniformly constrained to 0, ensuring the immobility of this end as well. However, a noteworthy exception is made in the Ux direction at this end, where an intentional 10 mm displacement has been applied. This prescribed displacement serves as a controlled deformation, strategically introduced to investigate the plate's response to such a directed force and provide valuable insights into its structural behavior under these dynamic conditions.

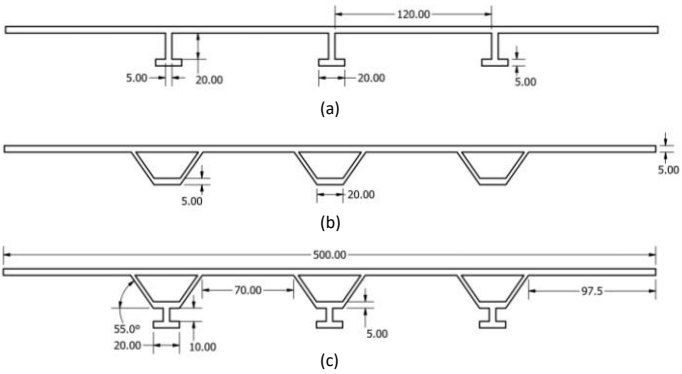

Fig. 3. The configurations and dimensions for the optimization of the train roof. These include (a) the T-type, (b) the Hat-type, and (c) the T-Hat type panels, with measurements provided in millimeters (mm).

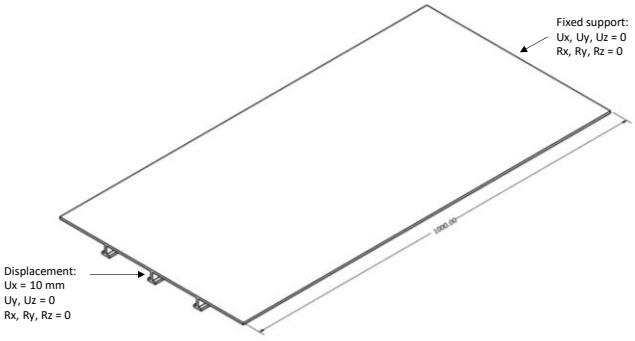

Fig. 4. The boundary conditions applied to the stiffened panel when it experiences buckling behavior.

In order to further enhance and deepen our comprehensive understanding of the plate's behavior, it is imperative to meticulously consider and thoroughly evaluate the critical influence of its material properties, as these properties play an indispensable role in shaping the plate's mechanical characteristics. The plate, in this particular context, is meticulously engineered using an aluminum alloy with a well-defined set of material attributes, including a density of 2780 kg/m³, a Young's modulus measuring at 73.4 GPa, a Poisson's ratio of 0.33, and a yield stress rating of 315 MPa. These meticulously specified material properties wield considerable significance, making a substantial contribution to the plate's overall mechanical response and therefore holding paramount importance in any structural analysis or design endeavor related to the plate.

4 Results and discussions

4.1 Force-Displacement

In the results and discussion of the buckling analysis of stiffened panels used in train roof structures, the data uncovers significant variations in the buckling behavior for different panel types. The T-type stiffened panel displayed a maximum buckling force of 702.0 kN at a displacement of 21.922 mm, while the Hat-type panel exhibited a maximum force of 875.33 kN at a displacement of 13.235 mm. Simultaneously, the T-Hat type panel registered the highest force of 1173.4 kN at a displacement of 16.434 mm, Fig. 5.

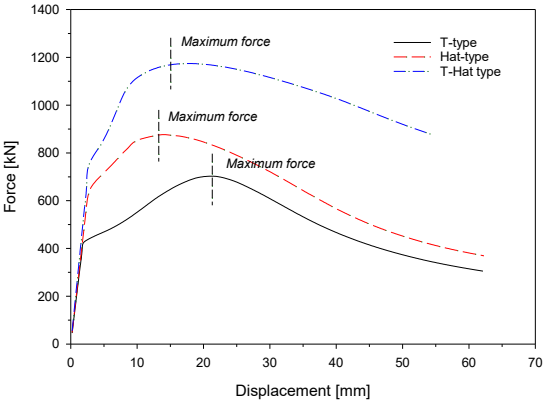

Fig. 5. Force versus displacement curve.

Maximum force can be used to determine the strength of the structure by assessing its ability to withstand the most extreme pressures and stresses [20]. To gain a deeper insight into these findings, the percentage differences between the maximum forces and displacements of the three panel types were calculated. The T-Hat type panel, in

particular, showcased the highest buckling force, with a percentage difference of approximately 67.5% compared to the T-type panel and 34.0% compared to the Hat-type panel. In contrast, the Hat-type panel exhibited the lowest percentage difference, approximately 19.7%, when compared to the T-type panel.

In practical applications, these insights hold great significance when designing train roof structures. The T-Hat type panel, with its notably higher buckling force, becomes a favorable choice for areas burdened with heavy loads or exposed to extreme conditions, thus enhancing structural integrity and safety. Conversely, the Hat-type panel emerges as a more suitable option in regions with less stringent requirements, where its lower weight and less pronounced buckling behavior offer cost-effective solutions while maintaining satisfactory performance. This analysis equips engineers with the knowledge to make informed decisions in selecting the most appropriate stiffened panel for specific train roof designs, thereby optimizing both performance and cost-efficiency [21].

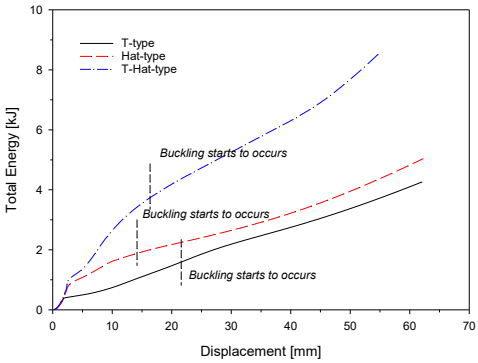

Fig. 6. Total generated energy versus displacement curve.

The comprehensive results obtained from the extensive buckling analysis of stiffened panels, specifically those designed for application in train roof structures, have unveiled a spectrum of total energy values that were encountered prior to the initiation of buckling phenomena. According to the data acquired during the study, it was discerned that the total energy demands for T-type panels amounted to 1.6188 kJ, while Hat-type panels exhibited a total energy requirement of 1.8263 kJ, and T-Hat type panels recorded a comparatively elevated total energy demand of 3.748 kJ, Fig. 6.

A deeper scrutiny of these findings unveiled a striking discrepancy, as T-Hat type panels exhibited a notably heightened total energy requirement for buckling, indicating a substantial 131.35% escalation when juxtaposed with the total energy levels observed in T-type panels. In a similar vein, these T-Hat type panels also displayed a considerable 105.29% increase in total energy demands when compared to the Hat-type panels. The implications of these results are pivotal in emphasizing the utmost importance of meticulously considering energy-related aspects in the design and en-

gineering of robust and resilient train roof structures, as they play an unequivocal role in their structural integrity and overall performance.

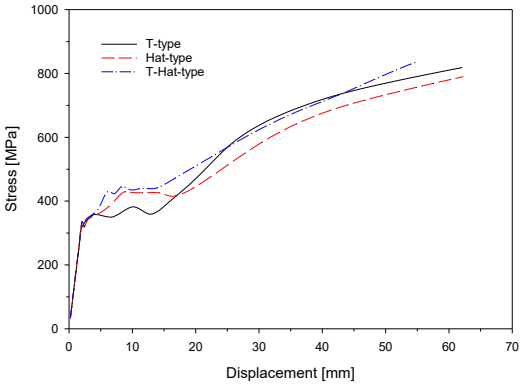

Fig. 7. Equivalent stress versus displacement curve.

The results and discussion of the buckling analysis for stiffened panels used in train roof construction reveal several findings. The data indicates that the stiffened panel's equivalent stress at the point of buckling initiation varies for different panel types: the T-type panel showed a value of 508.63 MPa, the Hat-type panel exhibited 426.79 MPa, and the T-Hat type panel had an equivalent stress of 468.92 MPa, Fig. 7. A previous study also confirmed that attaching different stiffener types to the plate affects stress concentration when subjected to a load, reinforcing our findings [20]. Calculating the percentage differences between these values, it is apparent that the T-type panel's equivalent stress is approximately 19.15% higher than that of the Hat-type panel, and the T-Hat type panel's equivalent stress is roughly 7.64% lower than that of the T-type panel but approximately 9.77% higher than that of the Hat-type panel. These findings provide insight into the structural performance and potential design considerations for stiffened panels in train roof applications.

4.2 Model Deformation

Fig. 8 shows the contour of Von-Misses stress. To analyze the von-Mises stress in the stiffened plate under a buckling load, it is needed to compare the stress values for different configurations: T = 818.73 MPa, Hat type = 790.25 MPa, and T-Hat type = 834.97 MPa. These values show a clear pattern: the T-Hat type stress has the highest magnitude, exceeding the Hat type stress by about 5.9%. The T stress is also very high, with a difference of about 4.3% from the Hat type stress. Fig. 8 shows the contour of von-Mises stress, which helps us understand how the stress is distributed in the stiffened plate. The areas with high stress concentrations in this figure are the most likely to fail, and they need more attention and improvement measures [19].

Fig. 9 presents the contour of total deformation. The buckling analysis results reveal different total deformation levels for each panel type. The T-type panel has a deformation of 62.11 mm, the Hat-type panel has 62.273 mm, and the T-Hat type panel has 54.647 mm. This means that the Hat-type panel deforms about 11.9% more than the T-type panel, while the T-Hat type panel deforms about 12.0% less than the Hat-type panel, indicating significant differences in how these panel designs respond structurally.

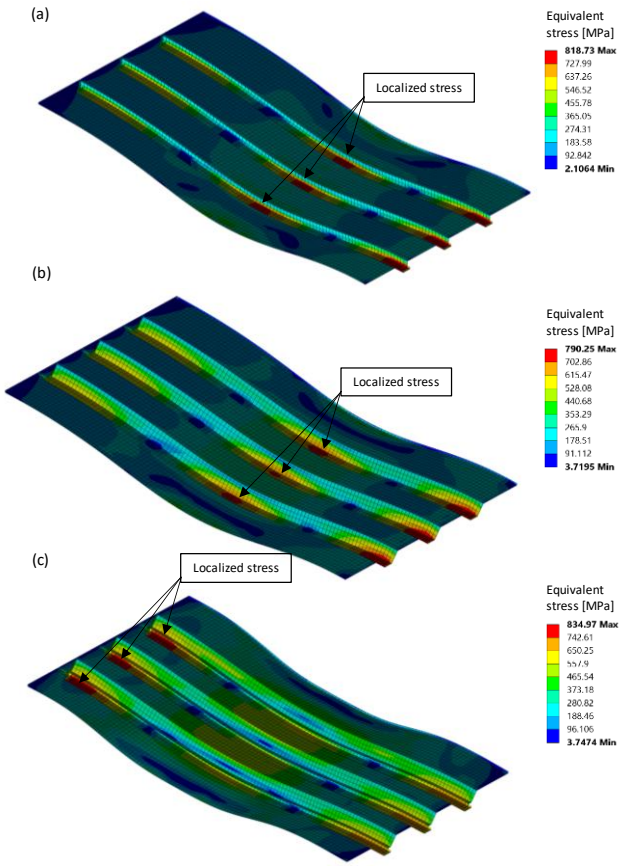

Fig. 8. The contour of Von-Misses stress that manifested following the occurrence of buckling. (a) the T-type, (b) the Hat-type, and (c) the T-Hat type panels.

Our study's stiffened panels underwent a thorough buckling analysis, which showed model deformations with equivalent plastic strain values of 0.011 for the T-type panel, 0.01 for the Hat-type panel, and 0.011 for the T-Hat type panel, Fig. 10. These results reveal important information about how the different panel designs behave under load. A closer look at these plastic strain values reveals a remarkable fact:

the Hat-type panel had the lowest plastic strain, with a percentage difference of about 9.09% lower than both the T-type and T-Hat type panels. Typically, the concentration of stress at this location resulted in extreme outcomes, such as the structural failure [19]. This finding highlights the possible benefits of the Hat-type panel design for structural strength and may have implications for future train roof design and optimization.

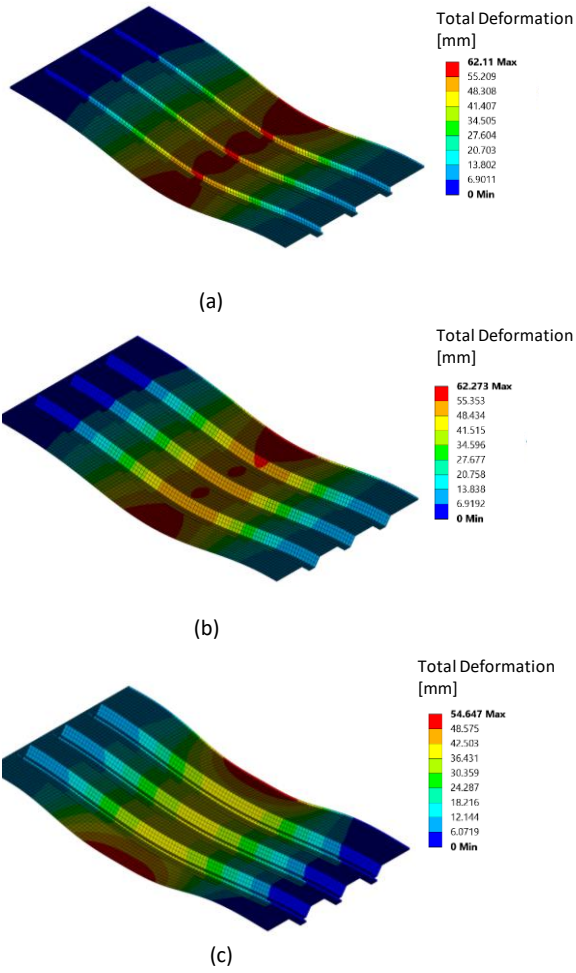

Fig. 9. The contour of total deformation that manifested following the occurrence of buckling. (a) the T-type, (b) the Hat-type, and (c) the T-Hat type panels.

One of the limitations of this study is that it does not account for the effects of the welding joining process on the buckling behavior of the train roof stiffened panel. The process of welding has the potential to create residual stresses, distortions, and defects, which can ultimately impact the structural integrity and stability of the panel

when subjected to external loads [22]. This, in turn, may result in severe and potentially disastrous failures [23-26]. Therefore, future studies should consider incorporating the welding process into the numerical and experimental analysis of the train roof stiffened panel under buckling load.

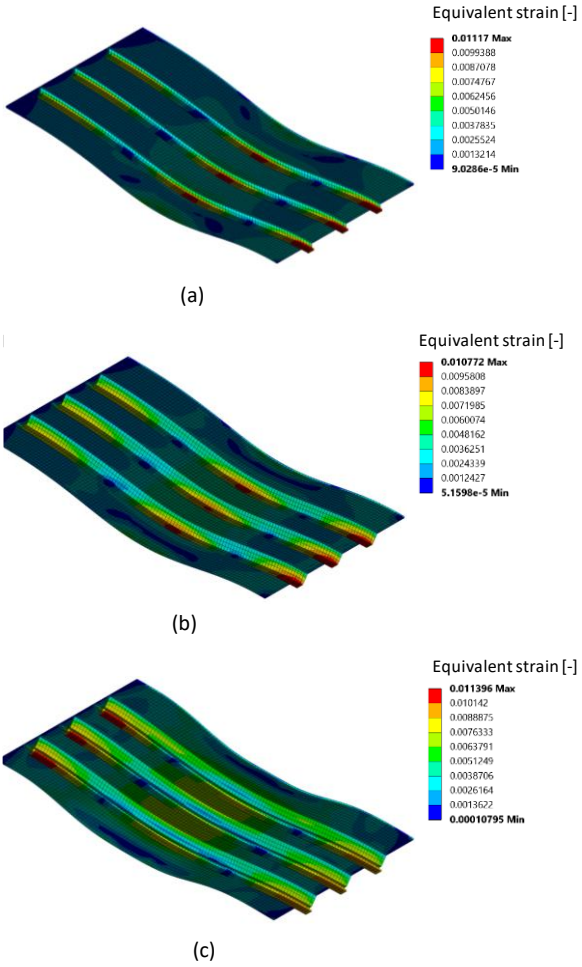

Fig. 10. The contour of equivalent plastic strain that manifested following the occurrence of buckling. (a) the T-type, (b) the Hat-type, and (c) the T-Hat type panels.

5 Conclusions

The study investigated a new design for train roof structures that can resist buckling under different loads. It compared three types of panels: T-Hat, Hat, and T. The T-Hat panel showed the best performance, with the highest buckling force and the largest

percentage difference from the other two panels. The Hat panel was better than the T panel, but not by much. These results can help improve the design and optimization of train roofs, especially the T-Hat panel design. However, this study did not consider how welding can affect the buckling behavior of the panels. Welding can cause stresses, distortions, and defects that may change how the panels behave under load. Future studies should include the welding process in the numerical and experimental analysis of the panels.

References

1. Wu, C., Zhang, N., Xu, L.: Travelers on the railway: An economic growth model of the effects of railway transportation infrastructure on consumption and sustainable economic growth. Sustain. 13, (2021).
2. Ridwan, R., Bacthiar, M., Ridwan, B., Prabowo, A.R.: An Overview of Railway Damage with the Finite. Adv. Eng. Res. 1, 3–12 (2023).
3. Rajkumar, R.I., Sankaranarayanan, P.E., Sundari, G.: An approach to Avoiding Train Collision in Railway Sectors Using Multi Agent System. Procedia Comput. Sci. 57, 1067–1073 (2015).
4. Yang, G., Bradford, M.A.: Thermal-induced buckling and postbuckling analysis of continuous railway tracks. Int. J. Solids Struct. 97–98, 637–649 (2016).
5. Ngamkhanong, C., Wey, C.M., Kaewunruen, S.: Buckling analysis of interspersed railway tracks. Appl. Sci. 10, (2020).
6. Bi, H., Zhou, Y., Wang, H., Gou, Q., Liu, X.: Characteristics of fire in high-speed train carriages. J. Fire Sci. 38, 75–95 (2020).
7. Crawford, E.G.C., Kift, R.L.: Keeping track of railway safety and the mechanisms for risk. Saf. Sci. 110, 195–205 (2018).
8. Reddy, J.N.: Theory and Analysis of Elastic Plates and Shells. Taylor & Francis Group, LLC, Boca Raton, Florida (2007).
9. Wang, C.M., Zhang, Y.P., Pedroso, D.M.: Hencky bar-net model for plate buckling. Eng. Struct. 150, 947–954 (2017).
10. Love, A.E.H.: The small free vibrations and deformation of a thin elastic shell. Proc. R. Soc. London. 43, 352–353 (1888).
11. Quinn, D., Murphy, A., McEwan, W., Lemaitre, F.: Stiffened panel stability behaviour and performance gains with plate prismatic sub-stiffening. Thin-Walled Struct. 47, 1457–1468 (2009).
12. ANSYS: Academic Research Mechanical, Help System, Coupled Field Analysis Guide; ANSYS Inc.: Canonsburg, PA, USA, 2023.
13. Esmaeili-Goldarag, F., Babaei, A., Jafarzadeh, H.: An experimental and numerical investigation of clamping force variation in simple bolted and hybrid (bolted-bonded) double lap joints due to applied longitudinal loads. Eng. Fail. Anal. 91, 327–340 (2018).
14. Goldarag, F.E., Barzegar, S., Babaei, A.: An experimental method for measuring the clamping force in double lap simple bolted and hybrid (bolted-bonded) joints. Trans. Famena. 39, 87–94 (2015).
15. Ridwan, R., Prabowo, A.R., Muhayat, N., Putranto, T., Sohn, J.M.: Tensile analysis and assessment of carbon and alloy steels using fe approach as an idealization of material fractures under collision and grounding. Curved Layer. Struct. 7, 188–198 (2020).
16. Prabowo, A.R., Ridwan, R., Tuswan, T., Imaduddin, F.: Forecasting the Effects of Failure Criteria in Assessing Ship Structural Damage Modes. Civ. Eng. J. 8, 2053–2068 (2022).

17. Prabowo, A.R., Tuswan, T., Prabowoputra, D.M., Ridwan, R.: Deformation of designed steel plates: An optimisation of the side hull structure using the finite element approach. Open Eng. 11, 1034–1047 (2021).
18. Prabowo, A.R., Ridwan, R., Tuswan, T., Sohn, J.M., Surojo, E., Imaduddin, F.: Effect of the selected parameters in idealizing material failures under tensile loads : Benchmarks for damage analysis on thin-walled structures. Curved Layer. Struct. 9, 258–285 (2022).
19. Ridwan, Putranto, T., Laksono, F.B., Prabowo, A.R.: Fracture and Damage to the Material accounting for Transportation Crash and Accident. Procedia Struct. Integr. 27, 38–45 (2020).
20. Prabowo, A.R., Ridwan, R., Muttaqie, T.: On the Resistance to Buckling Loads of Idealized Hull Structures: FE Analysis on Designed-Stiffened Plates. Designs. 6, 46 (2022).
21. Ghazijahani, T.G., Jiao, H., Holloway, D.: Longitudinally stiffened corrugated cylindrical shells under uniform external pressure. J. Constr. Steel Res. 110, 191–199 (2015).
22. Sudarno, S., Do, Q.T., Nubli, H., Prabowoputra, D.M., Dana, N.C.: Evaluating the Influence of Environmental Factors and Parameters on Advancements in Welding and Joining Processes : A Review. Maj. Ilm. Mek. 22, 88–100 (2023).
23. Ridwan, R., Sudarno, S., Nubli, H., Chasan, A., Istanto, I.: Numerical Analysis of Openings in Stiffeners under Impact Loading : Investigating Structural Response and Failure Behavior. Maj. Ilm. Mek. 22, 115–125 (2023).
24. Ridwan, R., Nuriana, W., Prabowo, A.R.: Energy absorption behaviors of designed metallic square tubes under axial loading : Experiment - based benchmarking and finite element calculation. J. Mech. Behav. Mater. 31, 443–461 (2022).
25. Prabowo, A. R., Tuswan, T., Ridwan, R.: Advanced development of sensors' roles in maritime-based industry and research: From field monitoring to high-risk phenomenon measurement. Appl. Sci. 11, 3954 (2021).
26. Alwan, F.H.A., Prabowo, A.R., Muttaqie, T., Muhayat, N., Ridwan, R., Laksono, F.B.: Assessment of ballistic impact damage on aluminum and magnesium alloys against high velocity bullets by dynamic FE simulations. J. Mech. Behav. Mater. 31, 595–616 (2022).